Electron. Mater. Lett., Vol. 10, No. 6 (2014), pp. 1109-1114
DOI: 10.1007/s13391-014-4114-6

Crystal Orientation Variation of Nonpolar AlN Films with III/V Ratio on *r*-Plane Sapphire Substrates by Plasma-Assisted Molecular Beam Epitaxy

Duc Duy Le, Dong Yeob Kim, and Soon-Ku Hong*

Department of Advanced Materials Engineering, Chungnam National University, Daejeon 305-764, Korea

(received date: 4 April 2014 / accepted date: 24 May 2014 / published date: 10 November 2014)

This paper reports the crystal orientation variation in the growth of nonpolar AlN films on *r*-plane sapphire substrates by plasma-assisted molecular beam epitaxy. The high III-V ratio growth condition (high Al flux) preferred single-crystalline *a*-plane AlN film growth, whereas the low Al flux condition resulted in the formation of an additional crystal orientation. The film grown under high III-V ratio growth condition also showed better crystal quality, as confirmed by x-ray diffraction rocking curve measurements. The *a*-plane AlN films with misoriented grains formed under lower Al flux showed growth recovery of single-crystalline *a*-plane AlN film with the increase in Al flux. The suspension of the misoriented structures in the AlN growth process by changing the Al flux implies a controllable transition of different orientations during the growth of nonpolar or semipolar III-nitrides.

Keywords: aluminum nitride, plasma-assisted molecular beam epitaxy, *r*-plane sapphire, crystal orientation control, non-polar III-V film

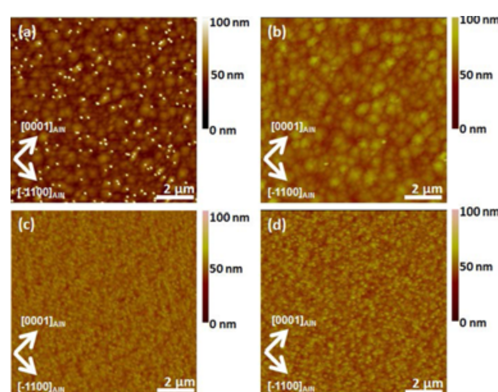

1. INTRODUCTION

Recently, group III-nitride materials have attracted much attention as promising materials for photoelectric devices.[1,2] As a material with large band gap energy among III-nitride group, aluminum nitride (AlN) stands out as a key component for devices working in ultra-short wavelength regimes.[3] Generally, AlN is grown on polar *c*-plane sapphire substrates, especially for commercial products. In *c*-plane AlN, a large internal electric field is induced along the [0001] direction because of spontaneous and piezoelectric polarization of wurtzite structure. This built-in electric field causes the intrinsic quantum-confined Stark effect, which reduces overlapping of electron and hole wave functions, thereby degrading the performances of devices like light-emitting devices (LEDs).[4,5] To eliminate this immanent property, nonpolar surfaces such as *m*-plane (10$\bar{1}$0 and *a*-plane (11$\bar{2}$0) of wurtzite semiconductors have been given considerable attention. Furthermore, due to the strong polarization, the nonpolar plane AlN LED shows strong emission along the surface normal, whereas the conventional *c*-plane AlN LED shows weak emission along the surface normal.[6] To achieve highly efficient photoelectric devices, studies on nonpolar AlN growth are necessary because of the suppression of built-in electrostatic fields in the polar direction.

The major concern for heteroepitaxially grown nonpolar films is crystallinity and microstructural defects. Defect formation is affected by several factors, including lattice misfit between film and substrate, different thermal expansion coefficients, growth conditions, gas flow rates, pressure, and substrate temperature.[7] Understanding the formation of lattice imperfections during film growth is an important key in improving film properties. Several reports showed that the crystallographic orientation of III-nitride films grown on *r*-plane sapphire substrates depends strongly on the dominant kinetic conditions during the growth of the first layers.[8,9] However, the variation of crystallographic orientation of *a*-plane III-nitride films during the growth process is not mentioned elsewhere. In this paper, we report the effects of III/V ratio on the growth and crystal structure orientation variation of nonpolar AlN films on *r*-plane sapphire substrate.

*Corresponding author: soonku@cnu.ac.kr
©KIM and Springer

2. EXPERIMENTAL PROCEDUCE

Nonpolar AlN films were grown on *r*-plane sapphire substrate by plasma-assisted molecular beam epitaxy (PAMBE). The commercial *r*-plane Al_2O_3 substrates were handled carefully over several steps to obtain clean substrates before the AlN growth processes. First, the substrates were degreased sequentially by ultrasonic agitation with acetone, methanol, and deionized (DI) water. The substrates were then etched with $H_2SO_4 : H_3PO_4 = 3 : 1$ (vol. %) mixture at 160°C for 15 min, followed by rinsing with DI water and drying under pure N_2 flow. After the chemical cleaning, the substrate was loaded in the growth chamber and thermally cleaned at 900°C for 20 min. The pressure of the growth chamber was maintained under 5×10^{-9} torr during the thermal cleaning. Prior to film growth, the substrates were nitrided at 860°C under nitrogen radiofrequency (RF) plasma. In the main AlN growth process, elemental Al (5N) and nitrogen RF plasma were used as group III and group V sources, respectively. The fluxes of Al were measured by a pressure-reading ion gauge at the substrate position as beam equivalent pressure (BEP). To study the role of Al flux condition, four samples of AlN film (S1, S2, S3, and S4) were grown on *r*-plane sapphire substrates by changing the Al fluxes, while the nitrogen flow rate and RF power were maintained at 0.76 sccm and 150 W. The growth process for the sample S4 involved two steps with different Al fluxes (BEP), that is, 2.3×10^{-7} torr in the first step and 2.7×10^{-7} torr in the second step. All of the films have thickness of about 300 nm. The growth conditions are presented in Table 1.

Growth procedures were *in-situ* monitored by reflection high-energy electron diffraction (RHEED). The surface morphology of the AlN films was investigated using an atomic force microscope (AFM) in tapping mode. The crystal quality of AlN films was characterized by x-ray omega rocking curves (XRC) for on-axis $(11\bar{2}0)$ reflection and for off-axis $(10\bar{1}1)$ reflections. The thickness of the films was evaluated from the cross-sectional images obtained using a scanning electron microscope (SEM). To investigate the film microstructure, cross-sectional transmission electron microscope (TEM) observation was performed by using a JEOL JEM 3011 HR operating at 300 keV. TEM sample was prepared via tripod wedge polishing method, followed by Ar^+ ion milling for electron transparency.

3. RESULTS AND DISCUSSION

The corresponding RHEED patterns of samples S1 to S4 observed at 12 and 24 min after the growth start are shown in Fig. 1. The main epitaxial growth relationships were estimated as $[11\bar{2}0]$ Al_2O_3//$[1\bar{1}00]$AlN, $[1\bar{1}01]$ Al_2O_3// [0001] AlN, which is consistent with other reports.[9-11] In this general epitaxial growth model of *a*-plane AlN on *r*-plane sapphire, three unit-cells of *a*-AlN may fit in one unit cell of *r*-plane sapphire. The theoretical lattice mismatch is calculated to be −2.8% and 13.1% in $[1\bar{1}01]$ and $[11\bar{2}0]$ directions of sapphire, respectively. In the sample S1 grown with an Al BEP of 2.3×10^{-7} torr, additional spots (marked by circles) were observed from 5 min to 8 min after the growth start, and were maintained until the growth end. The appearance of additional spots in the RHEED pattern indicates that there were misoriented crystallites formed at that growth time and those misoriented crystallites extended to the top of the *a*-plane AlN layers. On the other hand, additional spots in the RHEED pattern were not observed from the samples S2 and S3 (under the higher Al flux growth condition than that of sample S1) for the entire growth procedure. The RHEED patterns exhibited single crystalline characteristics without mixture of any other misoriented crystallites throughout the growth time [Figs. 1(b) and 1(c)]. Based on the RHEED observations, a close relationship was found between the formation of misoriented structures and the III-V ratio in growing AlN films by PAMBE.

To investigate the effect of Al flux on the formation of misoriented structures, sample S4 was grown and investigated by *in situ* RHEED. The sample S4 growth process involved two separate steps. The growth condition for the initial 12 min (first step) was the same as that for sample S1, but the consecutive 12 min (second step) was the same as that for sample S3. The RHEED results showed the variations of crystal structure similar to that in sample S1 in the first step. The additional spots were found in the RHEED images at 12 min. However, in the second growth step, the additional spots have been blurred quickly after the increase in Al flux. The single-crystal feature RHEED patterns of *a*-plane AlN remained until the end of the growth process [Fig. 1(d)]. As being seen from *in-situ* RHEED observations, the suppression of the misoriented crystallites in *a*-plane AlN occurred in

Table 1. Growth condition of samples S1, S2, S3, and S4.

Sample	S1	S2	S3	S4	
# of growth step	1 step	1 step	1 step	2 steps	
				1st step:	2nd step:
BEP_{Al} ($\times 10^{-7}$ torr)	2.3	2.5	2.7	2.3	2.7
Nitrogen plasma	Power: 150 W, Nitrogen flow rate: 0.76 sccm				
Growth time (min)	24	24	24	12	12

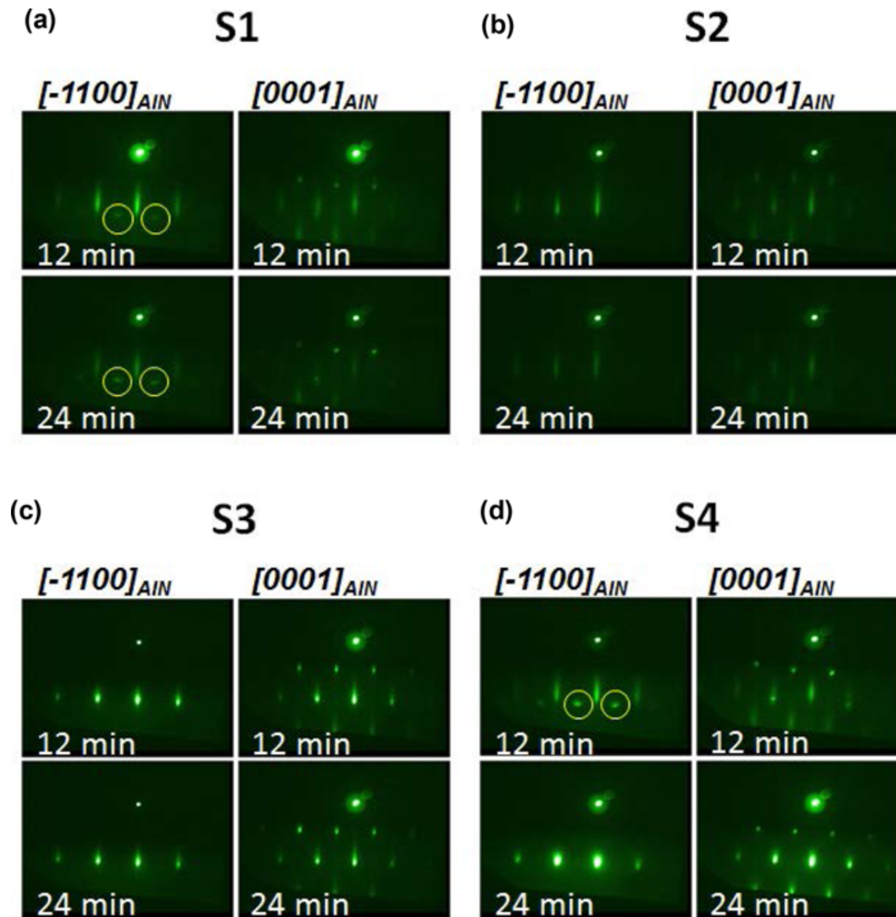

Fig. 1. RHEED patterns of the samples at 12 and 24 min of growth for (a) sample S1, (b) sample S2 (c) sample S3, and (d) sample S4. The growth conditions for each sample are presented in Table 1.

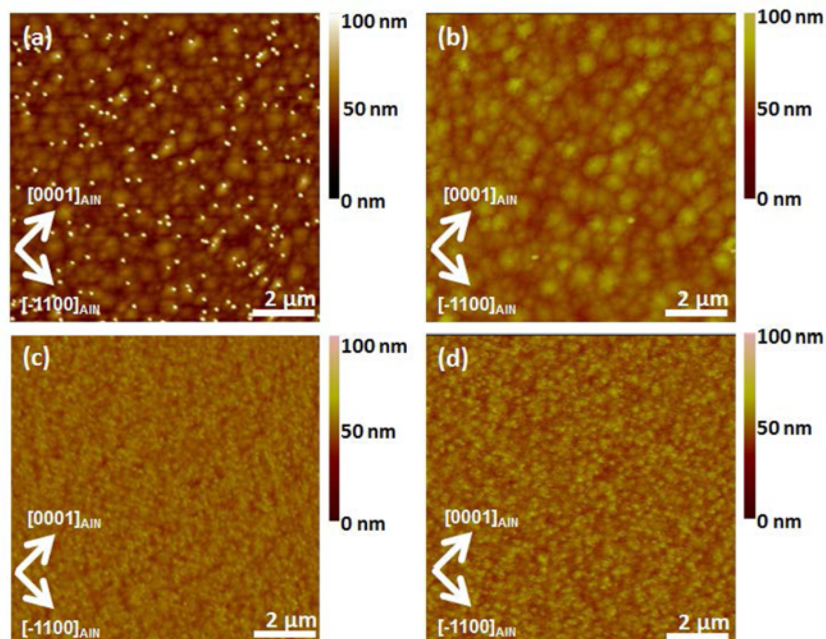

Fig. 2. AFM images of samples S1, S2, S3, and S4 grown under different Al flux conditions. The observed area is 10 μm × 10 μm.

high Al flux condition.

Figure 2 shows the AFM images of the samples observed from 10 × 10 μm^2 areas. The samples exhibit fully coalesced pit-free and striation-free surface morphology with low root-mean-square (RMS) roughness. Sample S1 showed granule-like morphology, which indicated columnar structure. Bright and small seed-like additional features were observed in sample S1, which may be responsible for the additional spots observed in the RHEED patterns in Fig. 1(a). Except for the additional seed-like morphology, sample S2 showed a morphology that was similar to that of sample S1. Sample S3 showed very flat surface morphology compared with samples S1 and S2, and possessed smaller granules. Sample S4 showed similar morphology to sample S3, implying that the final surface morphology was mostly affected by the applied growth condition. The RMS roughness observed from 10 × 10 μm^2 areas changed from 8.49 nm in sample S1 to 6.5 nm in sample S2 and 2.9 nm in sample S3. The roughness decreased almost three times as the Al flux increased. The decrease in RMS roughness can be due to the reduced migration of Al because high Al flux reduced migration of Al atoms on the surface of the film during the growth process. For sample S4 grown via the two-step method, the RMS roughness was about 4.1 nm, which was approximately between the value of sample S1 and S3.

Crystal quality of these samples was further characterized by XRC. The full width at half maximum (FWHM) values for both ($11\bar{2}0$) and ($1\bar{1}01$) reflections decreased with the increase in Al flux, as shown in the XRC curves in Fig. 3. The FWHM values of the AlN films were 1.544°, 1.473°, and 1.143° for off-axis ($1\bar{1}01$) reflection and 1.123°, 1.099°, and 0.916° for on-axis ($11\bar{2}0$) reflection for samples S1, S2, and S3, respectively. For sample S4, the FWHM XRCs were 1.227° and 0.935° for ($1\bar{1}01$) and ($11\bar{2}0$) reflections. These values were better than those of samples S1 and S2, but slightly worse than those of sample S3. It means that the crystal quality of sample S4 can be improved after changing the Al flux in the second step of growth.

To investigate the microstructure of sample S4 grown via the two-step method, cross-sectional TEM observation was carried out. Figure 4(a) is the low-magnification bright-field cross-sectional TEM image of sample S4 with [$1\bar{1}00$] AlN zone-axis. Figures 4(b) and 4(c) show the selected area electron diffraction patterns from some regions of sapphire substrate and AlN, respectively. For AlN, the diffraction pattern shows single-crystalline feature. Figure 4(d) shows the diffraction pattern obtained at the sapphire/AlN interface. In some regions of AlN, Moiré-like fringe is found, indicating an overlap of orient-different grains [Fig. 4(e)]. In the selected area electron diffraction pattern of this region, additional diffraction spots are found [marked by a circle in Fig. 4(f)]. Figure 4(g) is the corresponding dark-field image for the encircled spot in Fig. 4(f), showing misoriented grain, as supported by the RHEED observation. The forming region of the misoriented grain is about 50 nm to 150 nm above the AlN-sapphire interface (5 min to 12 min of the first growth step). In Fig. 4(g), the width of misoriented grain is about 50 nm to 70 nm. However, by changing the Al-flux in the second growth step, the misoriented grain shrunk and buried inside the *a*-plane oriented AlN layer. As a result, the uppermost layer of the AlN film in sample S4 remained only *a*-plane-oriented AlN. Based on the RHEED and TEM results, the misoriented grains prefer to be formed under low Al flux growth conditions. These misoriented grains can be suppressed and eliminated completely under high Al-flux condition in this study.

The growth of AlN, GaN, and InN films with different crystallographic orientations has been previously achieved on *r*-plane sapphire substrates.[8,9,12,13] In those reports, the III-V condition of the first buffer layer and vicinal *r*-plane substrates resulted in different main film crystal orientations on the same substrate. In the current study, we showed that the growth of nonpolar orientation can be changed by slightly changing the source flux during the growth processes.

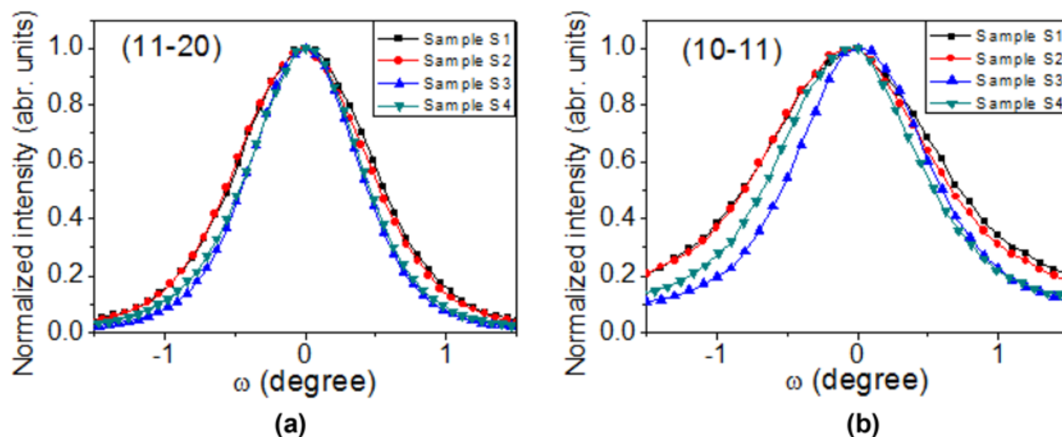

Fig. 3. XRCs of (a) on-axis ($11\bar{2}0$) reflections and (b) off-axis ($1\bar{1}01$) reflection.

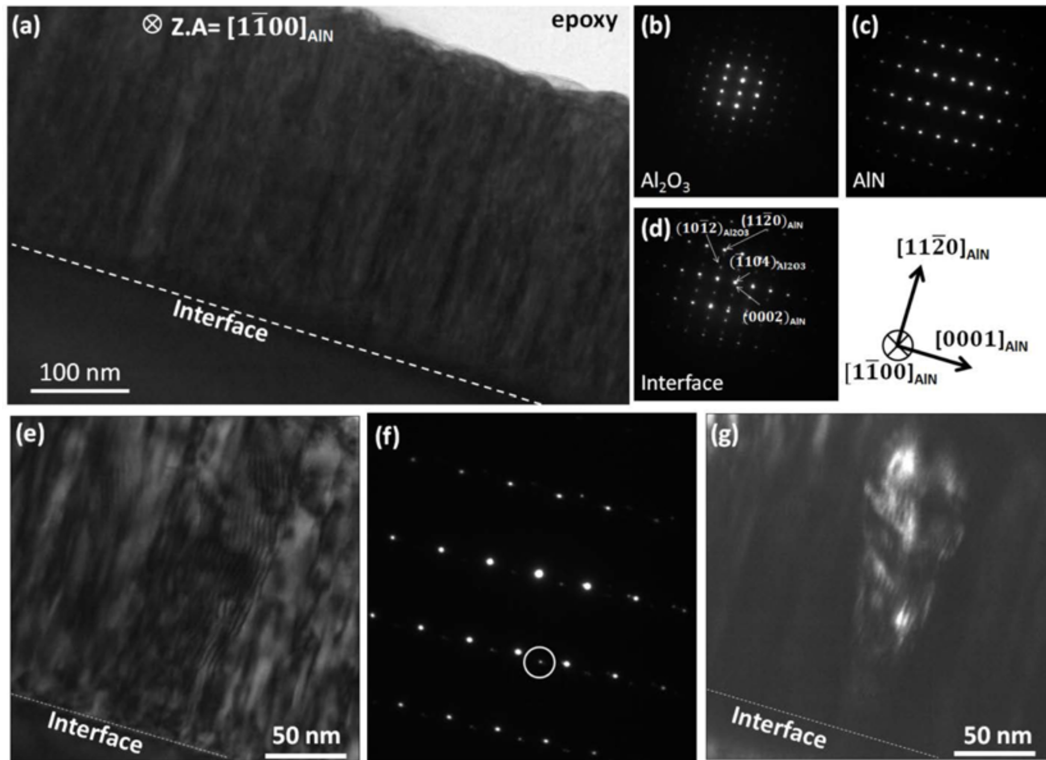

Fig. 4. (a) Bright-field low-magnification cross-sectional TEM image with the incident beam parallel to the [1$\bar{1}$00] of the *a*-plane-oriented AlN layer of sample S4. Selected area electron diffraction patterns of (b), a region of sapphire substrate, (c) a region of AlN film, and (d) the sapphire/AlN interface. (e) Magnified bright-field image showing Moiré-like fringe region and (f) the corresponding selected area electron diffraction pattern with additional diffraction spots (one of the spots is encircled). (g) Dark-field image obtained from the encircled spot in (f).

4. CONCLUSIONS

Several nonpolar [11$\bar{2}$0] AlN films with pit-free, and striation-free surface morphology were successfully grown on *r*-plane sapphire. The higher Al flux, the smoother surface and also the better crystallinity of AlN films were attained. The Al flux conditions remarkably affected the formation of the misoriented grain inside the *a*-plane AlN films. Under the given growth conditions in this study, the misoriented grains were formed at low Al flux growth condition, which was confirmed by the additional spot found in the *in situ* RHEED observation. With the increase in Al flux, single-crystalline AlN films were grown without the misoriented grains. Interestingly, the *a*-plane AlN films with the misoriented grain structures formed under low Al flux showed growth recovery of single-crystalline *a*-plane AlN film with the increase in Al flux, as confirmed by the two-step growth method employing low and high Al fluxes. The suspension of the misoriented structures in the AlN growth process by changing the Al flux implies a controllable transition of different orientations during the growth of nonpolar or semipolar III-nitrides.

ACKNOWLEDGMENTS

This research was supported by the National Research Foundation of Korea (NRF) funded by the Ministry of Education and Science & Technology (MEST), Korea (Grant No. NRF-2011-0016137).

REFERENCES

1. B. T. Tran and E. Y. Chang, *Electron. Mater. Lett*. **9**, 705 (2013).
2. W. Lee and J. S. Kwak, *Electron. Mater. Lett.* **9**, 451 (2013).
3. J. Li, K. B. Nam, M. L. Nakarmi, J. Y. Lin, H. X. Jiang, P. Carrier, and S.-H. Wei, *Appl. Phys. Lett*. **83**, 5163 (2003).
4. F. Bernardini, V. Fiorentini, and D. Vanderbilt, *Phys. Rev. B* **56**, R10024 (1997).
5. E. T. Yu, X. Z. Dang, P. M. Asbeck, S. S. Lau, and G. J. Sullivan, *J. Vac. Sci. Technol. B Microelectron. Nanometer Struct*. **17**, 1742 (1999).
6. Y. Taniyasu and M. Kasu, *Appl. Phys. Lett*. **96**, 221110 (2010).
7. B. Gil, *Group III Nitride Semiconductor Compounds:*

Physics and Applications, Clarendon Press (1998).
8. R. Chandrasekaran, A. S. Ozcan, D. Deniz, K. F. Ludwig, and T. D. Moustakas, *Phys. Status Solidi C* **4**, 1689 (2007).
9. R. Chandrasekaran, T. D. Moustakas, A. S. Ozcan, K. F. Ludwig, L. Zhou, and D. J. Smith, *J. Appl. Phys*. **108**, 043501 (2010).
10. P. Vennéguès and Z. Bougrioua, *Appl. Phys. Lett*. **89**, 111915 (2006).
11. Y. Danylyuk, S. Perooly, M. Rahman, and G. Auner, *Phys. Status Solidi C* **2**, 2228 (2005).
12. T. Shibata, K. Asai, Y. Nakamura, M. Tanaka, K. Kaigawa, J. Shibata, and H. Sakai, *J. Cryst. Growth* **229**, 63 (2001).
13. J.-J. Wu, K. Okuura, K. Fujita, K. Okumura, H. Miyake, and K. Hiramatsu, *J. Cryst. Growth* **311**, 4473 (2009).